GEOPHYSICS, VOL. 72, NO. 5 (SEPTEMBER-OCTOBER 2007); P. SM177–SM184, 10 FIGS., 1 TABLE.
10.1190/1.2744234

An approach for 3D multisource, multifrequency CSEM modeling

R.-E. Plessix[1], M. Darnet[1], and W. A. Mulder[1]

ABSTRACT

We discuss a practical approach for multisource, multifrequency controlled-source electromagnetic (CSEM) modeling. The approach consists of an efficient iterative multigrid-based solver and an automatic gridding procedure. For a given frequency and a given source location, the automatic gridding procedure ensures that the computational grid is consistent with the discretization of the electromagnetic equations. The conductivity is mapped from the input grid onto the automatically defined computational grid by volume averaging. This mapping changes the conductivity representation. Volume averaging based on the logarithm of the conductivity provides the best result. When the stretching in the computational grid is moderate, we use a multigrid method based on full coarsening. However, when the stretching is more severe, we propose a more robust multigrid method based on semicoarsening. Numerical examples show the usefulness of this approach for survey design and scenario studies over complex heterogeneous structures, when the layered-earth assumption is not satisfactory.

INTRODUCTION

Over the last 10 years, controlled-source electromagnetic (CSEM) technology has become more and more popular in the oil and gas industry for deepwater exploration (Chave et al., 1991; Eidesmo et al., 2002; Constable, 2006). This technique has the potential to detect resistive zones in a conductive background — in particular, to detect resistive hydrocarbon reservoirs in a conductive earth. Usually, the data are interpreted in the frequency domain with the help of normalized plots (Ellingsrud et al., 2002). These normalized plots require the choice of a reference acquisition point, where the measurements are not influenced by the resistive zones. The interpretation of those plots may be difficult in the presence of several resistive regions at different depths. In complex geologic settings, a modeling study is often required to correctly interpret CSEM data (Mehta et al., 2005; Hoversten et al., 2006; Darnet et al., 2007). Three-dimensional modeling is recommended because CSEM responses correspond to near-field measurements of diffusive electromagnetic waves. In certain cases, a layered-earth approach can be considered. However, when the actual earth shows large lateral contrasts, the layered assumption may lead to an overestimation of CSEM responses (Hoversten et al., 2006), and it is not applicable when strong lateral variations exist, for instance, when the bathymetry varies rapidly.

The interpretation of CSEM data recorded over relatively complex geologic settings may require several tens of solutions of the diffusive electromagnetic equations in a 3D inhomogeneous earth. To be of practical use, the modeling of a survey should take as little time as possible and, at most, several hours on a medium-size computer cluster to allow for survey planning, scenario study, or inversion for resistivity. Electromagnetic equations can be solved either in the time domain or in the frequency domain. In the frequency domain, a first possible approach consists of an analytic approximation of the field solution through integrals (Hursan and Zhdanov, 2002). This approach is quite efficient in relatively simple geometries. However, it may be less applicable when several resistive regions are present, when the background is varying, and when the bathymetry is not flat. Zhdanov et al. (2006) have extended the integral-equation method to account for a complicated background. A second approach consists of a finite-difference or finite-element solution of the electromagnetic equations (Newman and Alumbaugh, 1999; Davydycheva et al., 2003; Mulder, 2006). This approach permits any type of earth geometry. In 3D space, this leads to the solution of a very large linear system. This system is generally solved by an iterative solver. The efficiency of the method relies on a good preconditioner. Aruliah and Ascher (2003), Bochev et al. (2003), and Mulder (2006) propose the use of a multigrid method. The (diffusive) electromagnetic equations can be solved approximately by a multigrid solver (Hiptmair, 1998), and the solution can serve as a preconditioner for a Krylov (conjugate-gradient type) iterative solver. We based our CSEM code on this scheme and called it multigrid code in this paper. For multifrequency, multisource CSEM modeling, we parallelized over sources and frequencies, but we did not parallelize the solver. To limit the memory requirements and to speed up the computation,

Manuscript received by the Editor November 22, 2006; revised manuscript received February 21, 2007; published online August 23, 2007.
[1]Shell International E&P, Rijswijk, the Netherlands. Email: reneedouard.plessix@shell.com; mathieu.darnet@shell.com; wim.mulder@shell.com.

the computational grid must be adapted to the source location and to the frequency. For practical use, this grid adaptation must be automatic. This is done in two steps. First, the spacing and the dimensions of the computational grid are determined from the minimum and average skin depths. Then, the mapping/interpolation of the conductivity onto the computational grid is carried out using volume averaging. The mapping modifies the model representation and may introduce a change in the response because we did not consider anisotropy and effective-medium theory (Davydycheva et al., 2003).

When the stretching of the grid is too severe, one multigrid cycle based on a full coarsening (Mulder, 2006) provides a less accurate solution of the electromagnetic equations, and the number of iterations increases significantly. A more robust solver is obtained when the multigrid method is based on semicoarsening and line relaxation (Jönsthövel et al., 2006). For land or shallow-water applications, where the grid is generally severely stretched to account for a thick air layer, this more robust approach improves the efficiency of the solver. This solver can also be used to build a time-domain response when the latter is computed by a Fourier transform after having computed the frequency responses over a large frequency band (Newman et al., 1986; Mulder and Slob, 2007).

In this paper, we briefly describe the main steps of the solver and explain the automatic gridding approach. We illustrate the usefulness of this method on deepwater CSEM examples. Then, the multigrid method based on semicoarsening and line relaxation is reviewed, and a shallow-water example is discussed. Finally, we draw some conclusions.

ELECTROMAGNETIC SOLVER

The electromagnetic fields satisfy Maxwell's equations, and, in the earth, the conductive current is given by Ohm's law. In the frequency domain, the second-order differential equation in the electric field reads,

$$\imath\omega\mu_0\tilde{\sigma}(\mathbf{x},\omega)\mathbf{E}(\mathbf{x},\omega) - \nabla\times\mu_r^{-1}(\mathbf{x})\,\nabla\times\,\mathbf{E}(\mathbf{x},\omega) = \mathbf{F}(\mathbf{x},\omega). \tag{1}$$

The source term $\mathbf{F}$ is equal to

$$\mathbf{F}(\mathbf{x},\omega) = \imath\omega\mu_0\mathbf{J}_s(\mathbf{x},\omega) + \nabla\times\,\mu_r^{-1}(\mathbf{x})\mathbf{M}_s(\mathbf{x},\omega). \tag{2}$$

Here, $\mathbf{E}$ is the electric-field vector; $\mathbf{J}_s$ is the current-source vector; $\mathbf{M}_s$ is the magnetic-source vector; μ_0 is the magnetic permeability in the air; μ_r is the relative permeability; $\tilde{\sigma}(\mathbf{x},\omega) = \sigma(\mathbf{x}) - \imath\omega\varepsilon(\mathbf{x})$, with σ the conductivity and ε the dielectric permittivity; and ω is the angular frequency. The magnetic field $\mathbf{H}$ is given by

$$\mathbf{H}(\mathbf{x},\omega) = \frac{1}{\imath\omega\mu_0\mu_r}\,\nabla\times\,\mathbf{E}(\mathbf{x},\omega). \tag{3}$$

Traditionally, equation 1 is solved with a primary/secondary formulation. The conductivity is decomposed into $\tilde{\sigma} = \tilde{\sigma}_0 + \tilde{\sigma}_1$. The primary field $\mathbf{E}_0$ satisfies

$$\imath\omega\mu_0\tilde{\sigma}_0(\mathbf{x},\omega)\mathbf{E}_0(\mathbf{x},\omega) - \nabla\times\mu_r^{-1}(\mathbf{x})\nabla\times\,\mathbf{E}_0(\mathbf{x},\omega) = \mathbf{F}(\mathbf{x},\omega), \tag{4}$$

and the secondary field $\mathbf{E}_1$ satisfies

$$\imath\omega\mu_0\tilde{\sigma}(\mathbf{x},\omega)\mathbf{E}_1(\mathbf{x},\omega) - \nabla\times\mu_r^{-1}(\mathbf{x})\nabla\times\,\mathbf{E}_1(\mathbf{x},\omega) = -\,\imath\mu_0\tilde{\sigma}_1(\mathbf{x},\omega)\mathbf{E}_0(\mathbf{x},\omega). \tag{5}$$

The total field is equal to $\mathbf{E}_0 + \mathbf{E}_1$.

This primary/secondary formulation is relevant when the primary field $\mathbf{E}_0$ can be efficiently computed. This is the case if σ_0 is layered, because an analytical solution exists (Ward and Hohmann, 1988). This formulation allows us to treat the source singularity analytically, and, therefore, the gridding of the model for the finite-difference or finite-element scheme does not require specific care at the source point. From a practical point of view, a layered model should be defined. This can be a cumbersome task when modeling a full survey with multiple sources. A layered model per source location is required when the source depth varies, which is the case during a CSEM survey with a nonflat bathymetry. Therefore, we did not consider the primary/secondary formulation.

In our implementation, equation 1 is discretized with the finite-integration technique (Weiland, 1977; Clemens and Weiland, 2001). At the boundaries of the computational model, we use perfectly electrically conducting boundary conditions, namely $\mathbf{E}\times\mathbf{n} = 0$, with $\mathbf{n}$ the normal to the boundary. This leads to a linear system of the form

$$\mathbf{AE} = \mathbf{F}, \tag{6}$$

where $\mathbf{A}$ is the discrete Maxwell operator, $\mathbf{E}$ is the vector of the discrete values of the electric components, and $\mathbf{F}$ is the source vector. $\mathbf{A}$ is a large and non-Hermitian, but symmetric, sparse matrix, which can be solved by an iterative method. We implemented the method with the BICGSTAB2 scheme (Van der Vorst, 1992; Gutknecht, 1993). Without an efficient preconditioner, the number of iterations to reach convergence can be large. Newman and Alumbaugh (1999) used a massively parallel implementation to obtain a reasonable run time. With modern computer processors with few gigabytes of memory and an efficient preconditioner, the parallelization of the solver is no longer needed. A good preconditioner is obtained when one multigrid cycle is applied to approximately invert system 6 (Mulder, 2006). To illustrate the efficiency of the solver described in Mulder (2006), we have computed the electrical field at 0.25 Hz for the model displayed in Figure 1 on an AMD Opteron 2.2 GHz with 8 GB of memory. The three components are plotted in Figure 1. The model is discretized in x and y, with a constant spacing of 100 m. In the vertical direction z, the spacing varies from 10 to 50 m; this is required to represent the bathymetry variations, the hydrates, and the reservoir zone. To avoid edge effects, we added extra boundary layers of about 5 km in the x- and y-directions and at the bottom of the model. We also added a 50-km air layer on the top of the model with a conductivity of 10^{-10} S/m. The computational grid contains over 19 million grid points (273 by 273 by 253). The solver requires about 7.4 GB of memory because of the extra arrays needed by the multigrid and the BICGSTAB2 methods. Convergence, down to 10^{-5}, is reached after 25 BICGSTAB2 iterations and took about 140 minutes. In this computation, the grid was oversampled because a spacing of 100 m corresponds to more than 1/5 of the minimum skin depth. No specific refinement of the grid at the source was made. In the section, "Deepwater CSEM applications" below, we show that the computational time can be reduced with a grid spacing adapted to the frequency.

GRIDDING APPROACH

Although the iterative solver preconditioned with one multigrid cycle is rather efficient even with an oversampled grid, the memory requirements can be reduced if the computational grid is adapted to the source location and to the frequency. Eventually, this grid adaptation may speed up the code. As pointed out by Hoversten et al. (2006), the use of a 3D finite-difference code may be difficult, because the grid should be correctly chosen to get a good answer in a reasonable amount of time. When the source depth and the bathymetry are varying, it will be too cumbersome and impractical to ask the user to define a model per source and per frequency. We have, therefore, automated the gridding. However, we should keep in mind that a modification of the model representation may change the responses because we only consider isotropic modeling.

The grid adaptation consists of interpolating the model parameters $\mathbf{m}$, i.e., the conductivity, defined on an input grid $\mathcal{U}$ to a computational grid $\mathcal{C}$. A grid is defined as the Cartesian tensor product $\mathbf{x}_g \otimes \mathbf{y}_g \otimes \mathbf{z}_g$, where $\mathbf{x}_g$ (respectively, $\mathbf{y}_g$, $\mathbf{z}_g$) is an array of positions in x-direction (respectively, y- and z-direction). The spacing in each direction is not necessarily uniform, but only structured grids are considered. The vector $\mathbf{m}$ defines the values of the model parameters in each cell. Given $\mathbf{m}^{\mathcal{U}}$, the model vector on the input grid, the model vector $\mathbf{m}^{\mathcal{C}}$ on the computational grid is simply defined by the projection/interpolation operator $\mathbf{P}^{\mathcal{CU}}$:

$$\mathbf{m}^{\mathcal{C}} = \mathbf{P}^{\mathcal{CU}}\mathbf{m}^{\mathcal{U}}. \tag{7}$$

The grid adaptation can be split into two steps: the definition of the computational grid $\mathcal{C}$ and the interpolation of $\mathbf{m}^{\mathcal{U}}$ on $\mathcal{C}$. Notice that this grid adaptation is a priori valid for any solver.

In the earth, the electromagnetic waves are diffusive, and one of the main notions is the skin depth, δ:

$$\delta = \sqrt{\frac{2}{\omega\mu_0\mu_r\sigma}}. \tag{8}$$

The skin depth is the distance over which the amplitude of the electromagnetic waves is reduced by $e^{-1} \simeq 0.37$. In a homogeneous medium, the quasistatic approximation of equation 1 reduces to a Helmholtz equation with a complex wavenumber $k = \sqrt{\imath\omega\mu_0\mu_r\sigma} = (1 + \imath)/\delta$. It may be interpreted as a wave equation with a very large damping or viscous term (Løseth et al., 2006). A wavelength can be defined as 2π divided by the real part of the wavenumber, so the wavelength is equal to $2\pi\delta$. The discretization of equation 1 with the finite-integration technique (Clemens and Weiland, 2001) or with the finite-difference Yee scheme (Yee, 1966) gives a second-order scheme. With a wave equation, about 15 to 20 points per wavelength are required for a second-order scheme. Applying the same rule means about two to three points per skin depth. This gives a rule to automatically determine the spacing $d_\delta(f)$ at a frequency f:

$$d_\delta(f) = \frac{\delta_{\min}(f)}{r_\delta}, \tag{9}$$

with $\delta_{\min}$ the minimum skin depth and r_δ a number between two and three. For deepwater CSEM applications, the minimum skin depth occurs in the water where $\sigma \simeq 3.3$ S/m and $\delta_{\min}(f) \simeq 275/\sqrt{f}$.

Because we don't use the primary/secondary formulation, the grid should be refined at the source point to better approximate the fields around that point. With a source dipole of length L_s, we define the spacing d_s at the source point by

$$d_s = \min\left(\frac{L_s}{r_s}, d_\delta(f)\right), \tag{10}$$

with r_s a number generally between two and four. Numerically, we model the source line by a set of points along the line. We use the adjoint of the trilinear interpolation to distribute the point to the grid edges. This corresponds to the discretization of a Dirac; a narrow Gaussian could also be used. This source discretization allows us to model any dipole orientation.

The grid dimensions can be estimated from the average skin depth δ_{ave}. This average skin depth generally corresponds to the skin depth in the sediment zones, i.e., $\delta_{\text{ave}} \simeq 700/\sqrt{f}$ for a conductivity of 0.5 S/m. The computational domain is often decomposed into a core domain and extra boundary layers. The extra boundary layers are added to avoid edge effects. The core of the computational domain is defined as follows:

$$[x_s - r_x\delta_{\text{ave}}, x_s + r_x\delta_{\text{ave}}] \times [y_s - r_y\delta_{\text{ave}}, y_s + r_y\delta_{\text{ave}}] \times [z_{\text{air}}, z_s + r_z\delta_{\text{ave}}],$$

with r_x and r_y numbers between four and eight, depending on the location of the receivers, r_z a number around four, z_{air} the depth of the air-water interface, and $\mathbf{x}_s = (x_s, y_s, z_s)$ the midpoint of the source line. The thickness of the boundary layer, except in the air, is $t_b = r_b\delta_{\text{ave}}$, with r_b a number around four, and an air layer of about $t_a \simeq 50$ km is added. The numbers r_x, r_y, r_z, and r_b are chosen in this way because the amplitudes of the electromagnetic waves are reduced by 98% over four skin depths and by 99.97% over eight skin depths.

In the core of the computational domain, the gridding starts at $\mathbf{x}_s$, and power-law stretching is used to limit the number of points. To avoid too large numerical errors, the spacing is limited by $d_\delta(f)$. For instance, for the points in the x-direction at the right of $x_s = x_0$, this gives $x_i = x_{i-1} + \min(s_c^i d_s, d_\delta(f))$. Here, s_c is the stretching parameter taken equal to about 1.04. A relatively small stretching is used, be-

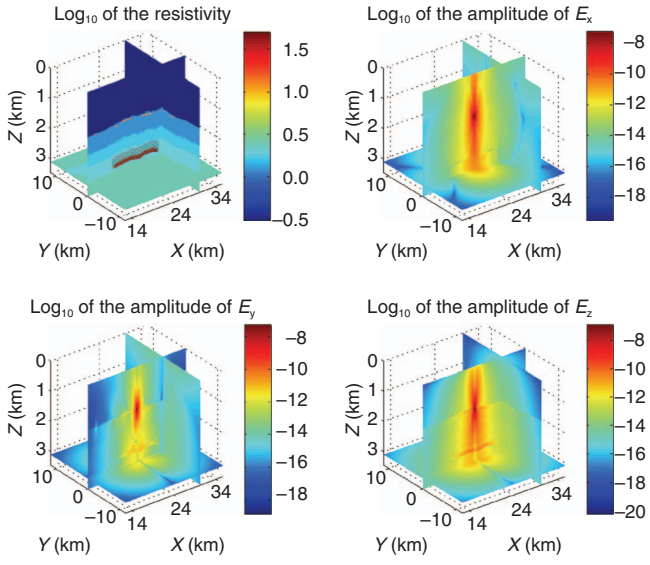

Figure 1. A large modeling example from deepwater Sabah. The source is a 270-m dipole in x, centered at $x = 24$ km, $y = 0$ km, $z = 1.4$ km. The computational grid has 273 by 273 by 257 (i.e., over 19 million with about 60 million unknowns) grid points. The frequency is 0.25 Hz. The resistivity is plotted on a logarithm scale.

cause the efficiency of the solver generally deteriorates with large stretching (Mulder, 2006). In the boundary layers, the grid is simply stretched with a power law: $x_i = x_{i-1} + s_b(x_{i-1} - x_{i-2})$, with $s_b \simeq 1.1$.

With the finite-integration technique (Weiland, 1977; Clemens and Weiland, 2001), theoretically, it is not needed to interpolate the model parameters onto the computational grid. The discretization is based on the integral form of Maxwell/Ohm's equations, and an integration scheme that takes into account the variations of the conductivity inside the integration domain can be implemented. This approach is not considered here. Instead, we decided to define a constant value per cell of the computational grid and to use the volume-average technique to interpolate the resistivity or the conductivity. This approach works nicely with smooth models. When the models contain discontinuities, the responses are modified because of the differences in the model representation, as will be illustrated by the numerical examples.

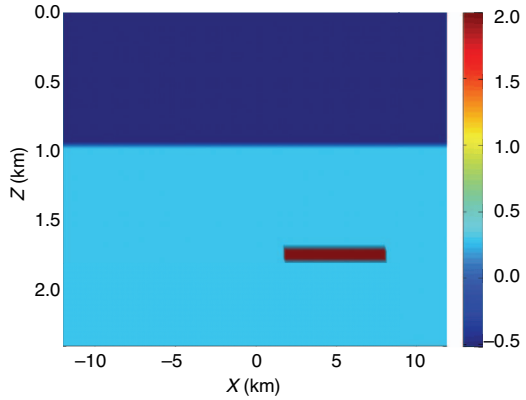

Figure 2. The resistivity of the simple model on a logarithm scale.

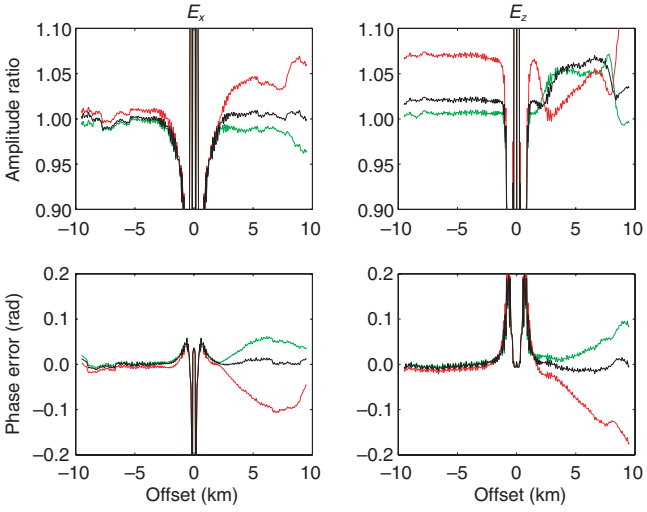

Figure 3. Amplitude ratios and phase differences at 0.25 Hz between the inline (E_x) and the vertical (E_z) components computed on the fine grid and on the adapted grid, in green when the volume averaging is carried out on the conductivity, in red when it is carried out on the resistivity, and in black when it is carried out on the logarithm of the conductivity.

DEEPWATER CSEM APPLICATIONS

To evaluate whether our approach is satisfactory to model CSEM surveys, several numerical examples are now presented. Comparisons are made with results obtained with the quasi-analytical code developed by Utah University in the CEMI consortium and based on the contraction integral-equation method (Zhdanov et al., 2000; Hursan and Zhdanov, 2002; Zhdanov et al., 2006). In these examples, the computational grid generation is controlled by $r_\delta = 3$, $r_s = 3$, $r_x = r_y = 8$, $r_z = 4$, and $r_b = 4$.

A simple example

The first example consists of a 1000-m water column and a 2 ohm-m homogeneous-earth background with a 100 ohm-m and 100-m-thick resistive zone at 700 m below the seafloor. The resistivity is plotted on a logarithm scale in Figure 2. The input grid is a relatively fine grid at 0.25 Hz, with a spacing of 150 m in x and y and 50 m in z. In the simulation, the midpoint of the 270-m horizontal electric-dipole source is at $(0,0,1)$ km, and the receiver line is at $y = 0$ and $z = 0.95$ km. To determine the conductivity field on the adapted grid, we carried out three different types of volume averaging: on the conductivity (green line in Figure 3), on the resistivity (red line), or on the logarithm of the conductivity (black line). Using the results on the (fine) input grid as a reference, the differences in amplitudes and phases of the responses obtained on the adapted grid are plotted in Figure 3. The interpolation modifies the amplitude responses of the inline (E_x) component by less than 5% and the responses of the vertical (E_z) component by a bit more than 5%. The phases vary by less than 0.1 radian, except when the averaging is carried out on the resistivity. The best results are obtained when the averaging is carried out on the logarithm of the conductivity. The amplitude variations are larger on the vertical component. The vertical electric field is discontinuous at the horizontal interfaces, and the interpolation tends to smooth the interfaces. This smoothing, therefore, modifies the amplitudes at the receivers that are close to the horizontal water-earth interface by a few percent. In order to limit

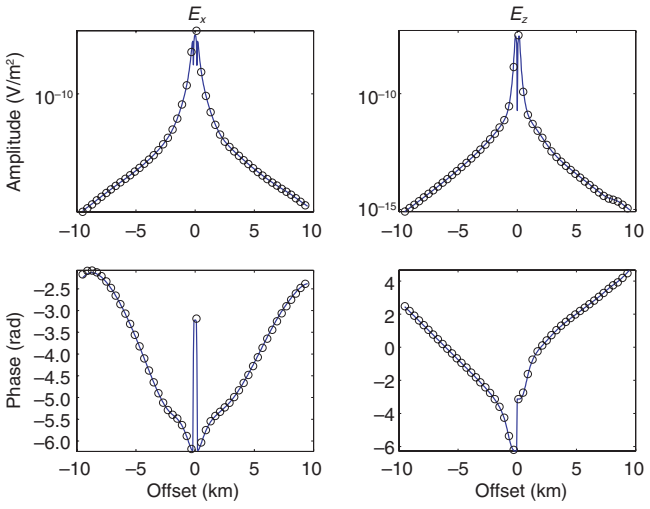

Figure 4. Comparison of the 0.25 Hz electric responses for the simple model. The inline (E_x) and vertical (E_z) components were computed with the multigrid code on the adapted grid after averaging of the logarithm conductivity (solid line) and computed with the quasi-analytical code (circle).

this smoothing effect, the spacing in z at the source depth can be set to 50 m instead of d_s. In Figure 4, we display the responses at 0.25 Hz obtained with the quasi-analytical code called INTEM3D (Zhdanov et al., 2000; Hursan and Zhdanov, 2002) and the ones obtained with the multigrid code and the adapted grid after averaging on the logarithm of the conductivity. In Figure 5, we display the responses at 7.25 Hz. The responses are very similar; the amplitude differences are a few percent, and the phase differences are around 0.1 rad. The adapted grid including the boundary layers contained $153 \times 153 \times 127$ points, and the code took about 500 s. The responses with the quasi-analytical code were obtained in 20 s.

Deepwater Sabah model

The second example is a more realistic example based on a real case from deepwater Sabah, offshore Malaysia (Darnet et al., 2007). The resistivity is displayed on a logarithm scale in Figure 1. The model contains a shallow resistive zone (hydrates) with a thickness of 10 to 20 m and deep resistive zones corresponding to a reservoir with a thickness varying between 10 to 50 m. The bathymetry, displayed in Figure 6, varies significantly. The 270-m inline electric-dipole source is located at (24,0,1.4) km. The receiver positions are represented by the black crosses in Figure 6. The input grid is a fine grid with a 100-m spacing in x and y and a 10–50-m spacing in z. The shallow and deep resistives zones are discretized with a 10-m spacing in z.

The first computations are carried out for a homogeneous earth below the varying bathymetry. This allows us, in a simple way, to also compare the results with the quasi-analytical code called PIE3D (Zhdanov et al., 2006). The responses obtained at 0.25 Hz with the quasi-analytical code (in black circle) and with the multigrid code after averaging on the logarithm of the conductivity (solid line) are plotted in Figure 7. The quasi-analytical code runs in about 30 min and requires more than 7 GB of memory; the multigrid-based code with the $157 \times 157 \times 105$ adapted grid runs in about 500 s and takes less than 2 GB of memory. Those results are obtained on a single processor. This illustrates that the multigrid code with a careful grid definition is a competitive approach for solving the electromagnetic equations in the deepwater CSEM context.

In Figure 8, we compare the results obtained with the multigrid code on the adapted grid with the ones obtained on the fine input grid. The computations are now carried out on the full model with shallow hydrates and deeper reservoirs (Figure 1). The conclusions are similar to those drawn in the simple example. The amplitudes of the inline electric component are modified by a few percent by the change in the model representation after averaging on the logarithm of the conductivity, and the phase differences are around 0.1 rad. For scenario studies or inversion, those differences are quite acceptable because it is considered that a resistivity anomaly should be larger than 10% to be detectable in a reliable manner. The differences are larger for the vertical component that is discontinuous at the water-earth interface. In this approach, we did not consider effective-medium theory because we consider only isotropic modeling. More precise results should be obtained if anisotropic modeling is used (Davydycheva et al., 2003). In Figure 9, the interpolated-resistivity

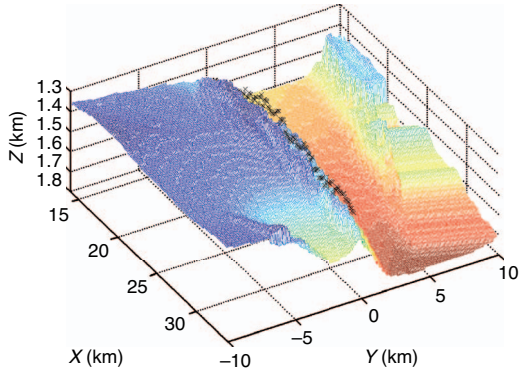

Figure 6. The bathymetry of the deepwater Sabah model. The receiver locations are represented by the black crosses.

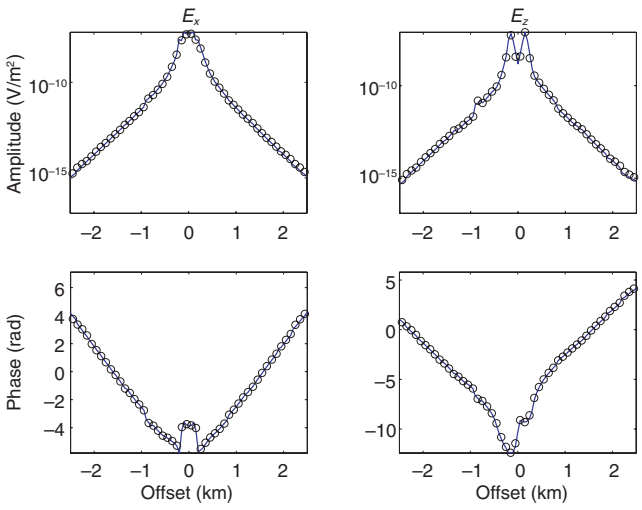

Figure 5. Comparison of the 7.25 Hz electric responses on the simple model. The inline (E_x) and vertical (E_z) components were computed with the multigrid code on the adapted grid after averaging of the logarithm conductivity (solid line) and computed with the quasi-analytical code (circle).

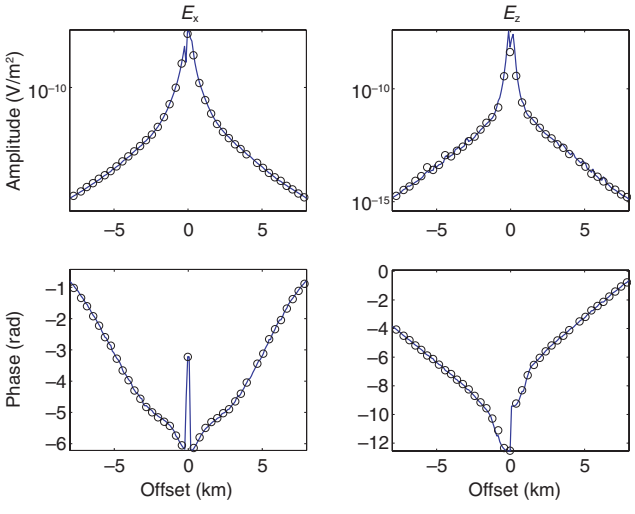

Figure 7. The inline (E_x) and vertical (E_z) components on the deepwater Sabah model with homogeneous earth conductivity. The electric fields were computed at 0.25 Hz with the multigrid code on the adapted grid after averaging of the logarithm conductivity (solid line) and computed with the quasi-analytical code (circle).

model and the electric-field components are displayed. A visual comparison with Figure 1 shows that the field responses are quite similar, although the model representation is different.

Finally, a full survey of 30 sources with two frequencies at 0.25 and 7.25 Hz was computed. Eleven AMD Opteron 2.2 Ghz processors were used. The code was parallelized over sources and frequencies with a master-slave approach. This means that the actual computation was carried out on 10 (slave) processors, and that communication occurs only between the master processor and the slave processors. The modeling of the full survey, which includes 60 forward-modeling runs, took less than 1 hour.

SHALLOW-WATER APPLICATIONS

With severe grid stretching, the number of iterations may become quite large. A more robust method was proposed in Jönsthövel et al., (2006), based on line relaxation and semicoarsening. Here, we will briefly describe the main differences with the original scheme and present convergence results for one example.

The multigrid method computes an approximate solution to the discretized equations by employing several grids simultaneously. Starting from the original fine grids, several coarser grids are defined. In our case, material properties are defined in cells. The electric-field components live on the midpoints of the edges of these cells in such a way that the direction of the component is parallel to the edge (Yee, 1966; Weiland, 1977; Clemens and Weiland, 2001). In the standard multigrid approach (Mulder, 2006), eight fine-grid cells are combined into a single coarse-grid cell, thereby halving the number of cells in each coordinate direction.

A relaxation scheme should compute an approximate solution on each grid. Relaxation schemes are typically efficient in computing the short-range, oscillatory, or rough components of the solution, but are inefficient for the long-range, smooth components. These smooth components can be represented on coarser grids, where they become oscillatory and are easily computed. In the multigrid context, the relaxation scheme should, therefore, determine the rough components of the solution. For that reason, it is often referred to as a smoother.

The residual, $\mathbf{F} - \mathbf{AE}$, measures how well an approximate solution obeys the discretized equation 6. After some smoothing steps, the residual can be projected onto a coarser grid. This projection is called restriction in the multigrid jargon. After restriction and some smoothing steps, we can project the resulting residual to a still coarser grid, until the number of cells is so small that a direct solver can be used.

Next, we have to interpolate the coarse-grid solution back to a finer grid. Since we used the restriction of the residual on the coarser grid, the coarse grid does not contain the full solution, but only a correction to the fine-grid solution. The interpolation of the coarse-grid correction to the finer grid is called prolongation.

In our case, the restriction operator is based on volume averaging, consistent with the discretization. The prolongation operator is its scaled adjoint. The relaxation scheme is symmetric *block Gauss-Seidel* (Arnold et al., 2000). This scheme selects a node and simultaneously solves for the six electric-field components that live on the edges attached to that node. Boundary nodes do not have to be visited because perfectly electrical conducting boundary conditions are used, meaning that the tangential components of the electric field are zero. The nodes are visited sequentially in what is called lexicographical ordering, using the most recent solution values available. This scheme is called *block Gauss-Seidel*. The symmetric variant is obtained by also traversing the grid in the reverse order, thereby doubling the computational effort.

The more robust scheme uses line relaxation. Instead of solving six electric-field components simultaneously, the electric-field components that live on all the edges connected to a line of interior nodes are treated at once. This results in a symmetric band, complex matrix $\mathbf{C}$ with 11 diagonals. Here, we should stress that $\mathbf{C}$ is not Hermitian. A Cholesky-type decomposition without pivoting is used to factor this matrix into $\mathbf{C} = \mathbf{L}\mathbf{L}^T$, where $\mathbf{L}$ is a lower-triangular matrix with

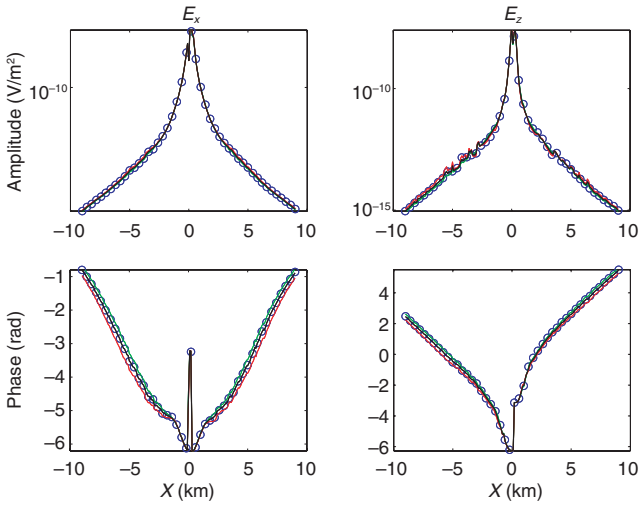

Figure 8. Electric responses at 0.25 Hz computed with the multigrid code on the deepwater Sabah model. The blue circles correspond to the values obtained on the fine grid, the red line on the adapted grid after averaging on the resistivity, the green line on the adapted grid after averaging of the conductivity, and the black line on the adapted grid after averaging of the logarithm of the conductivity.

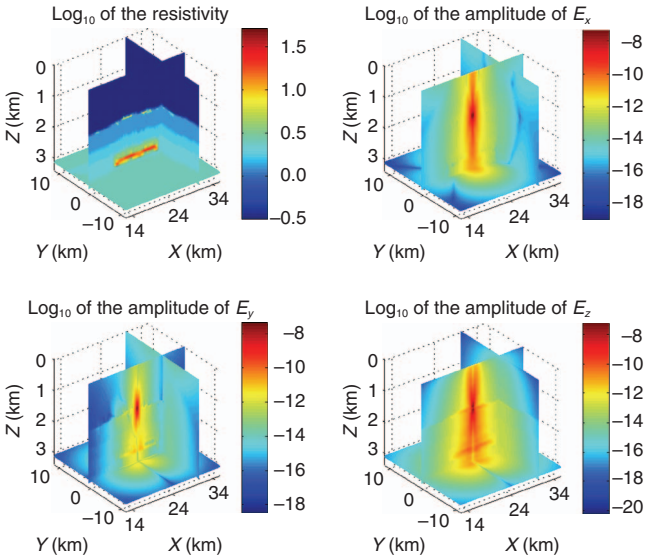

Figure 9. The electric fields computed at 0.25 Hz on the adapted grid of the deepwater Sabah model. The source is a 270-m dipole in x, centered at $x = 24$ km, $y = 0$ km, $z = 1.4$ km. The resistivity is plotted on a logarithm scale.

six diagonals, and T means transposition. Note that this approach is different from the standard Cholesky method for Hermitian matrices $\mathbf{B} = \mathbf{L}\mathbf{L}^*$, where $\mathbf{L}^*$, the adjoint of $\mathbf{L}$, equals the complex conjugate of the transpose of $\mathbf{L}$. The present Cholesky variant is about eight times faster than the generic line solver used in Jönsthövel et al. (2006). If one coordinate direction, say x, is selected for the line, the other two directions, y and z, can be traversed in lexicographical order. This scheme is called *line Gauss-Seidel*. Its symmetric variant, *symmetric line Gauss-Seidel* (SLGS), performs an additional sweep over y and z in the opposite order.

Another feature of the robust scheme is semicoarsening. Instead of combining eight cells into one when going to a coarser grid, we only combine four cells and keep the number of cells in one coordinate direction fixed.

Semicoarsening and SLGS were combined in the following way. We selected one coordinate direction, say x. The number of cells in that direction was kept constant during one multigrid cycle, so semicoarsening was applied in the y- and z-directions. At the same time, we applied SLGS in these two directions, both before restriction and after prolongation. For the next multigrid cycle, we choose the y-direction as having a constant number of cells and applied SLGS both in z and in x. Finally, the z-direction was not coarsened and SLGS acted in x and y. These three multigrid cycles were used as a single preconditioning step for BICGSTAB2 (Gutknecht, 1993). Because BICGSTAB2 involves two preconditioning steps, one full BICGSTAB2 iteration involves six multigrid cycles, compared to two in the original scheme. Note that BICGSTAB2 can be stopped after half an iteration.

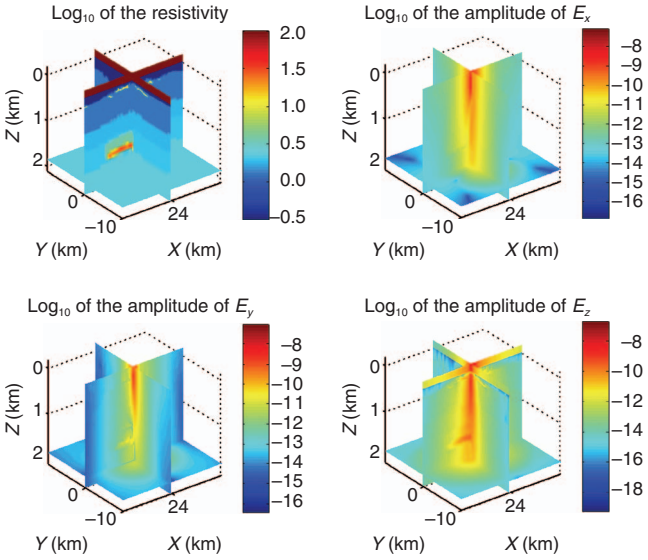

Figure 10. A shallow-water case. The electric fields were computed at 0.25 Hz. The source is a 270-m dipole in x, located at $x = 24$ km, $y = 0$ km, $z = 0.1$ km. The resistivity of the air is 10^{10} ohm-m. The plot of the logarithm of the resistivity is clipped at 100 ohm-m to keep the earth contrast visible.

Table 1. Number of BICGSTAB2 iterations and CPU-time ratio as a function of ε, the drop in the residual relative to that for a zero solution.

ε	Block	Line	CPU-time line/block
10^{-5}	38.5	1.0	0.32
10^{-6}	63.0	1.5	0.29

To illustrate the efficiency of the more robust method, we build a shallow-water example with 128^3 grid points from the deepwater Sabah model by removing about 1.2 km of water. In Figure 10, the resistivity model and the electric-field components are displayed. Table 1 lists the number of iterations and ratio of the central processing unit (CPU) times for the original and the robust scheme. The tolerance for convergence is ε. The iterations were stopped when $\|\mathbf{AE} - \mathbf{F}\| \le \varepsilon\|\mathbf{F}\|$. The robust scheme required very few iterations but each iteration, needed considerably more CPU time. Nevertheless, the scheme was about three times faster in this example. This more robust scheme is of little advantage for CSEM deepwater modeling where a moderate stretching is used. For land or shallow-water applications, where a thick air layer needs to be modeled, more severe stretching is often used to limit the memory requirements, and this robust scheme speeds up the code. This solver can also be used to compute the time-domain response. The approach then consists of computing the frequency responses over a large frequency band and finding the time response by a Fourier transform (Newman et al., 1986; Mulder and Solb, 2007).

CONCLUSIONS

We have presented an approach for multifrequency, multisource CSEM modeling in a 3D heterogeneous medium. The Maxwell/Ohm equations were discretized by the finite-integration technique. The linear system was solved by an iterative solver. The efficiency of the solver relies on a multigrid method to approximately estimate the solution of the electromagnetic equations. Given a frequency and a source location, an automatic gridding scheme based on the minimum and average skin depths has been described. The conductivity was mapped onto the computational grid by volume averaging. Averaging on the logarithm of the conductivity limits the differences caused by the change in the model representation to a few percent. For scenario studies or inversion, those small differences are quite acceptable.

When the stretching of the grid is moderate, the multigrid approach was based on a full coarsening. This implementation was used for deepwater applications, and the multigrid code on the adapted grid generally required several hundreds of seconds to compute a single-source, single-frequency response on a single processor. A multifrequency, multisource CSEM data set could, therefore, be generated in a couple of hours on a small computer cluster. This illustrates the relevance of this approach for scenario studies or survey design in complex geological settings. For shallow-water applications, more severe stretching is often required to model a thick air layer without increasing the memory requirements too much. The multigrid approach based on a full coarsening is then less efficient, and the number of iterations of the solver increases. A more robust multigrid approach is obtained with semicoarsening and line relaxation. This approach significantly reduces the number of iterations. On the shallow-water example, the computational time was divided by three, thanks to this more robust multigrid approach.

REFERENCES

Arnold, D. N., R. S. Falk, and R. Winther, 2000, Multigrid in H(div) and H(curl): Numerische Mathematik, **85**, 197–217.

Aruliah, D. A., and U. M. Ascher, 2003, Multigrid preconditioning for Krylov methods for time-harmonic Maxwell's equations in 3D: SIAM Journal on Scientific Computing, **24**, 702–718.

Bochev, P. B., J. J. Hu, A. C. Robinson, and R. S. Tuminaro, 2003, Towards robust 3D *Z*-pinch simulations: Discretization and fast solvers for magnetic diffusion in heterogeneous conductors: Electronic Transactions on Numerical Analysis, **15**, 186–210.

Chave, A. D., S. C. Constable, and R. N. Edwards, 1991, Electrical exploration methods for the seafloor, *in* M. Nabighian, ed., Electromagnetic methods in applied geophysics, vol. 2: SEG, 931–966.

Clemens, M., and T. Weiland, 2001, Discrete electromagnetism with the finite integration technique: Progress in Electromagnetic research, **32**, 65–87.

Constable, S., 2006, Marine electromagnetic methods — A new tool for offshore exploration: The Leading Edge, **25**, 438–444.

Darnet, M., M. C. K. Choo, R.-E. Plessix, M. L. Rosenquist, K. Yip-Cheong, E. Sims, and J. W. K. Voon, 2007, Detecting hydrocarbon reservoir from controlled source electromagnetic (CSEM) data in complex settings, Application to deep water Sabah, Malaysia: Geophysics **72**, no. 2, WA97–WA103.

Davydycheva, S., V. Druskin, and T. Habashy, 2003, An efficient finite-difference scheme for electromagnetic logging in 3D anisotropic inhomogeneous media: Geophysics, **68**, 1525–1536.

Eidesmo, T., S. Ellingsrud, L. M. MacGregor, S. Constable, M. C. Sinha, S. Johansen, and F. K. Kong, 2002, Seabed logging (SBL), a new method for remote and direct identification of hydrocarbon-filled layers in deep water areas: First Break, **20**, 144–152.

Ellingsrud, S., T. Eidesmo, S. Johansen, M. C. Sinha, L. M. MacGregor, and S. Constable, 2002, Remote sensing of hydrocarbon layers by seabed logging (SBL): Results from a cruise offshore Angola: The Leading Edge, **21**, 972–982.

Gutknecht, H. H., 1993, Variants of BiCGStab for matrices with complex spectrum: SIAM Journal on Scientific and Statistical Computing, **14**, 1020–1033.

Hiptmair, R., 1998, Multigrid method for Maxwell's equations: SIAM Journal on Numerical Analysis, **36**, 204–225.

Hoversten, G. M., A. G. Newman, N. Geier, and G. Flanagan, 2006, 3D modeling of a deepwater EM exploration survey: Geophysics, **71**, no. 5, G239–G248.

Hursan, G., and M. S. Zhdanov, 2002, Contraction integral equation method in three-dimensional electromagnetic modeling: Radio Science, **37**, 1089 , doi: 10.1029/2001RS00251.

Jönsthövel, T. B., C. W. Oosterlee, and W. A. Mulder, 2006, Improving multigrid for 3-D electro-magnetic diffusion on stretched grids, *in* P. Wesseling, E. Oñate, and J. Périaux, eds., Proceedings of ECCOMAS European Conference on Computational Fluid Dynamics: CDROM.

Løseth, L. O, H. M. Pedersen, B. Ursin, L. Amundsen, and S. Ellingsrud, 2006, Low-frequency electromagnetic fields in applied geophysics, Waves or diffusion?: Geophysics, **71**, no. 4, W29–W40.

Mehta, K., M. Nabighian, and Y. Li, 2005, Controlled source electromagnetic (CSEM) technique for detection and delineation of hydrocarbon reservoirs: An evaluation, 75th Annual International Meeting, SEG, Expanded Abstracts, 546–549.

Mulder, W. A., 2006, A multigrid solver for 3D electromagnetic diffusion: Geophysical Prospecting, **54**, 633–649.

Mulder, W. A., and E. C. Slob, 2007, TDEM by FDEM: Progress in Electromagnetics Research Symposium, 1794–1798.

Newman, G. A., and D. L. Alumbaugh, 1999, Electromagnetic modeling and inversion on massively parallel computers, *in* M. Oristaglio and B. Spies, eds., Three dimensional electromagnetics: SEG, 299–321.

Newman, G. A., G. W. Hohmann, and W. L. Anderson, 1986, Transient electromagnetic response of a three-dimensional body in a layered earth: Geophysics, **51**, 1608–1627.

Van der Vorst, H. A., 1992, BI-CGSTAB: a fast and smoothly converging variant of bi-CG for the solution of nonsymmetric linear systems: SIAM Journal on Scientific and Statistical Computing, **13**, 631–644.

Ward, S. H., and G. W. Hohmann, 1988, Electromagnetic theory for geophysical applications, *in* M. N. Nabighian, ed., Electromagnetic methods in applied geophysics — Theory, vol. 1: SEG, 131–311.

Weiland, T., 1977, A discretization method for the solution of Maxwell's equations for six-components fields: Electronics and Communications **31**, 116–120.

Yee, K., 1966, Numerical solution of initial boundary value problems involving Maxwell's equations in isotropic media IEEE Transactions on Antennas and Propagation, **16**, 302–307.

Zhdanov, M. S., V. I. Dmitriev, S. Fang, and G. Hursan, 2000, Quasi-analytical approximations and series in electromagnetic modeling: Geophysics, **65**, 1746–1757.

Zhdanov, M. S., S. K. Lee, and K. Yoshioka, 2006, Integral equation method for 3D modeling of electromagnetic fields in complex structures with inhomogeneous background conductivity: Geophysics, **71**, no. 6, G333–G345.